The two-component system ChvGI maintains cell envelope homeostasis in *Caulobacter crescentus*

Alex Quintero-Yanes[1], Aurélie Mayard[1] and Régis Hallez[1,2,$,#]

[1] *Bacterial Cell cycle & Development (BCcD), Biology of Microorganisms Research Unit (URBM), Namur Research Institute for Life Science (NARILIS), University of Namur, Namur (5000), Belgium*

[2] *WELBIO, University of Namur, Namur (5000), Belgium*

[$] *ORCID ID: 0000-0003-1175-8565*

[#]Corresponding author: Tel: +32 81 724 244; E-mail: regis.hallez@unamur.be

Running title: ChvGI-dependent cell envelope homeostasis

Key words: Two-component system, cell envelope, PBP, peptidoglycan, osmotic shock, mecillinam, cefsulodin, moenomycin, vancomycin

Abstract

Two-component systems (TCS) are often used by bacteria to rapidly assess and respond to environmental changes. The ChvG/ChvI (ChvGI) TCS conserved in α-proteobacteria is known for regulating expression of genes related to exopolysaccharide production, virulence and growth. The sensor kinase ChvG autophosphorylates upon yet unknown signals and phosphorylates the response regulator ChvI to regulate transcription. Recent studies in *Caulobacter crescentus* showed that *chv* mutants are sensitive to vancomycin treatment and fail to grow in synthetic minimal media. In this work, we identified the osmotic imbalance as the main cause of growth impairment in synthetic minimal media. We also determined the ChvI regulon and found that ChvI regulates cell envelope architecture by controlling outer membrane, peptidoglycan assembly/recycling and inner membrane proteins. In addition, we found that ChvI phosphorylation is also activated upon antibiotic treatment with vancomycin. We also challenged *chv* mutants with other cell envelope related stress and found that treatment with antibiotics targeting transpeptidation of peptidoglycan during cell elongation impairs growth of the mutant. Moreover, these antibiotics activate expression of the *chvIG-hprK* operon. Finally, we observed that the sensor kinase ChvG relocates from a patchy-spotty distribution to distinctive foci after transition from complex to synthetic minimal media. Interestingly, this pattern of (re)location has been described for proteins involved in cell growth control and peptidoglycan synthesis upon osmotic shock. Overall, our data support that the ChvGI TCS is mainly used to monitor and respond to osmotic imbalances and damages in the peptidoglycan layer to maintain cell envelope homeostasis.

41 **Importance**

42 The cell envelope is the first barrier protecting cells from harsh environmental
43 conditions, such as temperature, pH, oxidative and osmotic imbalances. It is also an
44 obstacle for the intake of antibiotics targeting essential cellular processes. Therefore,
45 molecular components and systems responding to cell envelope stress and
46 maintaining cell envelope homeostasis are important targets for drug therapy. Here
47 we show that the two-component system ChvGI, highly conserved in free-living and
48 pathogenic α-proteobacteria, is activated upon osmotic upshift and treatment with
49 antibiotics targeting peptidoglycan synthesis to activate the transcription of multiple
50 genes involved in cell envelope homeostasis in *Caulobacter crescentus*. We also
51 show that the kinase sensor ChvG displays a dynamic localisation pattern that
52 changes depending on osmotic imbalance. To our knowledge this is the first two-
53 component system reported to change his cellular localisation upon environmental
54 stress.

55 ## Introduction

56 Two-component systems (TCS) equip cells with a rapid sensing and response
57 mechanism to optimise survival in changing and stressful environments. The first
58 component of canonical TCS, a sensor histidine kinase (HK), autophosphorylates
59 upon input signal detection on a conserved histidine residue using the gamma-
60 phosphoryl group of ATP. Thereafter, the phosphoryl group is transferred from the HK
61 on a conserved aspartate residue of the second TCS component, a cognate response
62 regulator (RR). In most cases, the RR harbours an output domain that binds to DNA
63 upon phosphorylation to either activate or repress transcription of target genes (Stock
64 *et* al., 2000; Goulian, 2010; Capra & Laub, 2012). On the other hand, HKs can also
65 exert specific phosphatase activities on their RRs to turn off the response in absence
66 of the input signal (Gao and Stock, 2009).

67 The Chv (**ch**romosomal **v**irulence factor) TCS conserved in α-proteobacteria and
68 composed of the HK ChvG and the RR ChvI, was first reported as a pathogenic
69 regulator in *Agrobacterium tumefaciens* responding to acid stress (Mantis & Winans,
70 1993; Li *et al.,* 2002). A study in *Sinorhizobium meliloti* showed that the ChvG
71 homologue ExoS is negatively regulated by the periplasmic protein ExoR (Chen *et al.,*
72 2008). Further research in *A. tumefaciens* showed that low pH triggers ExoR
73 proteolysis to derepress ChvGI activity (Wu *et al.,* 2012). While unlike other α-
74 proteobacteria, ExoR orthologs are absent in the aquatic free-living bacterium
75 *Caulobacter crescentus*, the ChvGI-dependent response to acidic conditions seems
76 nonetheless conserved in *C. crescentus* (Stein *et al.,* 2021). Similarly, the ChvI
77 homologue BvrR of the intracellular pathogen *Brucella abortus* is phosphorylated in

78 combination of low pH and nutrient depletion conditions, which mimics post-infection
79 conditions (Altamirano-Silva *et al.,* 2018).
80 In *C. crescentus*, ChvGI activates the expression of the small non-coding RNA (sRNA)
81 ChvR when exposed to acidic stress or DNA damage with mitomycin C, or when
82 cultured in synthetic minimal media (Frölich *et al.,* 2018). Once produced, ChvR
83 subsequently inhibits translation of the TonB-dependent receptor (TBDR) ChvT
84 (Frölich *et al.,* 2018). Interestingly, inactivating of *chvR* or *chvIG* sensitises *C.*
85 *crescentus* cells to vancomycin treatment whereas a *chvT* mutant makes them
86 resistant to this antibiotic, which suggests that vancomycin passes through the outer
87 membrane via the TBDR ChvT to reach the periplasm (Vallet *et al.,* 2020). In addition,
88 a *chvIG* knock-out (Δ*chvIG*) mutant could not propagate in synthetic minimal media
89 when cells were inoculated at low density, while inactivating *chvT* in a Δ*chvIG*
90 background partially restored growth (Stein *et al.,* 2021). Although *chvIG* mutants are
91 sensitive to acid stress when grown in minimal media, the primary cause for the growth
92 defect has not been determined.
93 ChvGI is also known in *C. crescentus* to coordinate its regulation with another TCS,
94 NtrYX, which is under control of the periplasmic protein NtrZ (Stein *et al.,* 2021). NtrZ
95 has been only described in *C. crescentus*, while the HK NtrY and RR NtrX are known
96 for regulating multiple processes in α-proteobacteria such as nitrogen metabolism,
97 motility, virulence and cell envelope integrity (Pawlowski *et al.,* 1991; Carrica *et al.,*
98 2012; Wang, D *et al.,* 2013; Lemmer *et al.,* 2020). Stein *et al.* (2021) showed that both
99 ChvI and NtrX networks significantly overlap and these RRs have opposite regulatory
100 functions in minimal media. For instance, while ChvI acts as a positive regulator of
101 growth, NtrX inhibits growth. Interestingly, repression of growth in synthetic media is

102 caused by unphosphorylated NtrX, so that inactivating *ntrX* in a Δ*chvI* background also
103 partially restored growth. Actually, NtrY acts as a phosphatase over the
104 phosphorylated NtrX (NtrX~P), while NtrZ inhibits NtrY to presumably maintain high
105 NtrX~P levels.
106 Here we show that *chvIG* mutants are greatly impacted due to osmotic imbalances in
107 minimal media, but also in complex media supplemented with osmolytes. The
108 Although the general stress response (GSR) sigma factor SigT was shown to be
109 activated upon osmotic imbalance (Alvarez-Martinez *et al.*, 2007), we showed that
110 *chvIG* mutants are much more sensitive to lower hypertonic conditions than *sigT*
111 mutant. In agreement with previous data (Stein *et al.,* 2021), deletion of *chvT* and *ntrX*
112 restored growth in hypertonic conditions. We provide a ChvI regulon, using ChIP-seq
113 with polyclonal anti-ChvI antibodies and RNA-seq, which unveiled new targets related
114 to peptidoglycan (PG) synthesis and recycling. We also showed that (i) ChvG-
115 dependent phosphorylation of ChvI and (ii) expression of the *chvIG-hprK* operon is
116 induced upon osmotic shock or treatment with antibiotics targeting the PG. Finally, we
117 showed that upon these stressful conditions, the HK ChvG relocates from a patchy-
118 spotty pattern typically displayed by PG-related proteins to midcell. Overall, our results
119 support a critical role for the ChvGI TCS in maintaining cell morphology and cell
120 envelope homeostasis upon stress.
121

122 ## Methods

123 **Bacterial strains and growth conditions.**

124 Strains, plasmids and oligonucleotides used in this study are listed in supplementary
125 tables (Tables S 1, 2 and 3). Plasmid construction details are presented in
126 supplementary methods. *E. coli* strains were grown aerobically in either LB (broth)
127 sigma or LB + 1.5% agar at 37 ^{o}C. All *C. crescentus* strains in this study are derived
128 of the NA1000 wild-type strain, and growth was achieved at 30 ^{o}C in aerated conditions
129 using either complex medium Peptone Yeast Extract (PYE) or synthetic media
130 supplemented with glucose (M2G or M5GG) as already described in (Ronneau et al.,
131 2016). M2G and M5GG were prepared using M2 (12.25 mM Na_2HPO_4, 7.75 mM
132 KH_2PO_4, 9.35 mM NH_4Cl) and M5 (10 mM PIPES pH 7.2, 1 mM NaCl, 1 mM KCl, 0.37
133 mM Na_2HPO_4, 0.23 mM KH_2PO_4) salts, respectively, and both supplemented with (0.5
134 mM $MgSO_4$, 0.5 mM $CaCl_2$, 0.01 mM $FeSO_4$, 0.2% glucose). 1 mM glutamate sodium
135 was added to make M5GG. Modified M2G 0% (Na^+, K^+), M2G 25% (Na^+, K^+) and M2G
136 50% (Na^+, K^+) were prepared without Na_2HPO_4 and KH_2PO_4 or either 50% or 25% of
137 the Na_2HPO_4 and KH_2PO_4 concentrations in M2G, respectively. *C. crescentus* was
138 grown on plates using either PYE or M2G supplemented with 1.5% agar at 30 ^{o}C.
139 Growth was monitored by measuring absorbance at OD_{660} in liquid cultures using an
140 automated plate reader (Biotek, Epoch 2) with continuous shaking at 30 ^{o}C. Gene
141 expression under the control of inducible promoter (P_{xylX}) was induced either with 0.1
142 % D(+)-xylose (Sigma). Expression of enhanced green fluorescent protein (*egfp*) and
143 monomeric cherry (*mCherry*) protein fusions was induced in fresh exponentially
144 growing cultures (OD_{660} ~ 0.1) for 1 h and 4 h. Generalized transduction was
145 performed with phage ϕCr30 according to the procedure described in (Ely, 1991).

146 Antibiotics for *E. coli* were used with the following final concentrations (μg ml^{-1}, in
147 liquid/ solid medium) ampicillin (50/100), kanamycin (30/50), chloramphenicol (30/20),
148 and oxytetracycline (12.5/12.5) for *C. crescentus* A22 (2.5/5) cefsulodin (80/80),
149 cephalexin (15/15), mecillinam (100/100), moenomycin (0.5/1), kanamycin (5/20),
150 oxytetracycline (1/2.5), polymyxin B (5/12.5), vancomycin (10/10) where appropriate.
151 Plasmid delivery into *C. crescentus* was achieved by either bi- or tri-parental mating
152 using *E. coli* S17-1 and *E. coli* MT607 as helper strains, respectively. In-frame
153 deletions were created by using the pNPTS138-derivative plasmids as follows.
154 Integration of the plasmids in the *C. crescentus* genome after single homologous
155 recombination were selected on PYE plates supplemented with kanamycin. Three
156 independent recombinant clones were inoculated in PYE medium without kanamycin
157 and incubated overnight at 30 °C. Then, dilutions were spread on PYE plates
158 supplemented with 3% sucrose and incubated at 30 °C. Single colonies were picked
159 and transferred onto PYE plates with and without kanamycin. Finally, to discriminate
160 between mutated and wild-type loci, kanamycin-sensitive clones were tested by PCR
161 on colony using locus-specific oligonucleotides.
162
163 **Spotting assays**
164 Ten-fold serial dilutions (in PYE) were prepared in 96-well plates from 5 ml cultures in
165 standard glass tubes grown overnight at 30 °C in the corresponding media. Cells were
166 then spotted on plates, were incubated at 30 °C for two-to-three days and pictures
167 were taken. Cells in assays including strains with mutations in Δ*ntrX* were normalised
168 to OD_{660} since these mutations lead to growth defects in PYE.
169

170 **β-galactosidase assays**

171 β-galactosidase assays were performed as already described in Beaufay et al., 2015.
172 Briefly, overnight saturated cultures of *Caulobacter* cells harbouring *lacZ* reporter
173 plasmids were diluted ≥50X in fresh medium and incubated at 30 °C until OD_{660} of 0.3
174 to 0.5. 100 μl samples were collected in a 96 well plate and kept at -80 °C until
175 measurement. Then, 50 μl of aliquots of the previously frozen samples were thawed
176 and immediately treated with 50 μl Z buffer (60 mM Na_2HPO_4, 40 mM NaH_2PO_4, 10
177 mM KCl, 1 mM $MgSO_4$, pH 7.0) supplemented with 0.1 g polymyxin B and 0,27 % (v/v)
178 β-mercaptoethanol for 30 min at 28 °C. To this, 150 μl of Z buffer were added, followed
179 by 50 μl of 4 mg/ml O-nitrophenyl-β-D-galactopyranoside (ONPG). Then, ONPG
180 hydrolysis was measured at 30 °C for 30 min. The activity of the β-galactosidase
181 expressed in miller units (MU) was calculated using the following equation: MU =
182 (OD_{420} × 1,000) / [OD_{660} × t × v] where "t" is the time of the reaction (min), and "v" is
183 the volume of cultures used in the assays (ml). Experimental values were the average
184 of three independent experiments.

185

186 **Microscopy**

187 Strains grown in PYE were imaged either in exponential or stationary phase using 1.5
188 % agar pads with the indicated medium. Cells in osmotic shock conditions were
189 pelleted and washed twice with the indicated stress medium and imaged in 1.5 % agar
190 pads maintaining the stress condition. Images were obtained using Axio Imager Z1
191 microscope (Zeiss), Orca-Flash 4.0 camera (Hamamatsu) and Zen 2.3 software
192 (Zeiss). Temperature (30 °C) was maintained stable during microscopy analysis using
193 the Tempcontrol 37-analog 1 channel equipment (HemoGenix®) coupled to the Axio

194 Imager Z1 microscope. Images were processed with ImageJ. Demographs were
195 obtained with MicrobeJ by segmenting each cell, integrating fluorescence, sorting cells
196 by length and plotting fluorescence intensity and cellular widths to indicate the relative
197 position of the protein fusions, in which 0 represents mid-cell and 2 or -2 the cell poles
198 (Ducret *et al.*, 2016). Confocal microscopy images were obtained using a LSM900
199 Ayriscan microscope. Samples were prepared for imaging Fresh using cells grown to
200 OD_{660} 0.5. Cells were fixed immediately with a 12.5% paraformaldehyde and 150 mM
201 $NaPO_4$ solution. Cells were mixed gently and incubated for 15 min at room
202 temperature, then at 4 ^{o}C for 40 min. Then, cells were washed four times with 1.5X
203 volume of dH_2O. Cells were immobilized in CELLlview slides (Greiner bio-one) by
204 treating wells beforehand with 30 μl 0.1 % poly-L-lysine, then removing poly-L-lysine
205 by aspiration and hydrating wells with a drop water. Thereafter, 10 μl of cells were
206 added to the well and let to sit for 10 mins. Cells in suspension were aspirated and the
207 remain coated cells let to dry for 1 min. Finally, a drop of SlowFade™ Gold Antifade
208 Mountant (Thermo Fisher) was added to wells containing immobilised cells.
209

210 **Protein purification and production of polyclonal antibodies**

211 In order to immunize rabbits for production of ChvI polyclonal antibodies His6-ChvI
212 was purified as follows. A BL21(DE3) strain harboring plasmid pET-28a-*chvI* was
213 grown in LB medium supplemented with kanamycin until an OD_{600} of 0.7 was reached.
214 IPTG (isopropyl-β-D-thiogalactopyranoside) (Thermo Fisher Scientific) was added at
215 a final concentration of 1 mM, and the culture was incubated at 37 ^{o}C for 4 h. Then,
216 cells were harvested by centrifugation for 20 min at 5,000 *g* and 4 ^{o}C. The pellet was
217 resuspended in 20 ml BD buffer (20 mM Tris-HCl [pH 8.0], 500 mM NaCl, 10%

218 glycerol, 10 mM MgCl2, 12.5 mM imidazole) supplemented with complete EDTA-free
219 protease cocktail inhibitor (Roche), 400 mg lysozyme (Sigma), and 10 mg DNase I
220 (Roche) and incubated for 30 min on ice. Cells were then lysed by sonication and the
221 lysate cleared by centrifugation (12,000 rpm for 30 min at 4 °C) was loaded on a Ni-
222 nitrilotriacetic acid (Ni-NTA) column and incubated for 1 h at 4 °C with end-over-end
223 shaking. The column was then washed with 5 ml BD buffer, 3 ml Wash1 buffer (BD
224 buffer with 25 mM imidazole), 3 ml Wash2 buffer (BD buffer with 50 mM imidazole),
225 and 3 ml Wash3 buffer (BD buffer with 75 mM imidazole). Proteins bound to the
226 column were eluted with 3 ml elution buffer (BD buffer with 100 mM imidazole) and
227 aliquoted in 300 μl fractions. All the fractions containing the protein of interest (checked
228 by Coomassie blue staining) were pooled and dialyzed in dialysis buffer (50 mM Tris
229 [pH 7.4], 12.5 mM MgCl2). Purified ChvI was used to immunize rabbits (CER Groupe,
230 Marloie, Belgium).
231
232 **Immunoblot analysis**
233 Proteins crude extracts were prepared by harvesting cells from exponential growth
234 phase (OD_{660} ~ 0.3). The pellets were then resuspended in SDS-PAGE loading buffer
235 by normalizing to the OD_{660} before lysing cells by incubating them for 10 min at 95 °C.
236 The equivalent of 0.5 ml of cult (OD_{660} ~ 0.3) was loaded and proteins were subjected
237 to electrophoresis in a 12% SDS-polyacrylamide gel, transferred onto a nitrocellulose
238 membrane then blocked overnight in 5% (wt/vol) nonfat dry milk in phosphate buffer
239 saline (PBS) with 0.05% Tween 20. Membrane was immunoblotted for ≥ 3 h with
240 primary monoclonal anti-GFP (1:5,000) antibodies (JL8, Clontech-Takara), then
241 followed by immunoblotting for ≤ 1 h with secondary antibodies: 1:5,000 anti-mouse

242 linked to peroxidase (Dako Agilent), and vizualized thanks to Clarity™ Western ECL
243 substrate chemiluminescence reagent (BioRad) and Amersham Imager 600 (GE
244 Healthcare).
245
246 **Chromatin immunoprecipitation followed by deep sequencing (ChIP-Seq)**
247 **assay.**
248 A ChIP-Seq protocol was followed as described by Coppine *et al.* (2020). Briefly, 80
249 ml of mid-log-phase cells (OD_{660} of 0.6) were cross-linked in 1% formaldehyde and 10
250 mM sodium phosphate (pH 7.6) at room temperature (RT) for 10 min and then for 30
251 min on ice. Cross-linking was stopped by addition of 125 mM glycine and incubated
252 for 5 min on ice. Cells were washed twice in phosphate buffer solution (PBS; 137 mM
253 NaCl, 2.7 mM KCl, 10 mM Na_2HPO_4, 1.8 mM KH_2PO_4, pH 7.4) resuspended in 450 μl
254 TES buffer (10 mM Tris-HCl [pH 7.5], 1 mM EDTA, and 100 mM NaCl), and lysed with
255 2 μl of Ready-lyse lysozyme solution for 5 min at RT. Protease inhibitors (Roche) were
256 added, and the mixture was incubated for 10 min. Then, 550 μl of ChIP buffer (1.1%
257 Triton X-100, 1.2 mM EDTA, 16.7 mM Tris-HCl [pH 8.1], and 167 mM NaCl, plus
258 protease inhibitors) were added to the lysate and incubated at 37 °C for 10 min before
259 sonication (2 x 8 bursts of 30 sec on ice using a Diagenode Bioruptor) to shear DNA
260 fragments to a length of 300 to 500 bp. Lysate was cleared by centrifugation for 10
261 min at 12,500 rpm at 4 °C, and protein content was assessed by measuring the OD_{280}.
262 Then, 7.5 mg of proteins was diluted in ChIP buffer supplemented with 0.01% SDS
263 and precleared for 1 h at 4 °C with 50 μl of SureBeads Protein A Magnetic Beads
264 (BioRad) and 100 μg bovine serum albumin (BSA). One microliter of polyclonal anti-
265 ChvI antibodies was added to the supernatant before overnight incubation at 4 °C

266 under gentle agitation. Next, 80 μl of BSA presaturated protein A-agarose beads were
267 added to the solution and incubated for 2 h at 4 °C with rotation, washed once with
268 low-salt buffer (0.1% SDS, 1% Triton X-100, 2 mM EDTA, 20 mM Tris-HCl [pH 8.1],
269 150 mM NaCl), once with high-salt buffer (0.1% SDS, 1% Triton X-100, 2 mM EDTA,
270 20 mM Tris-HCl [pH 8.1], 500 mM NaCl), once with LiCl buffer (0.25 M LiCl, 1% NP-
271 40, 1% deoxycholate, 1 mM EDTA, 10 mM Tris-HCl [pH 8.1]), and once with TE buffer
272 (10 mM Tris-HCl [pH 8.1] 1 mM EDTA) at 4 °C, followed by and a second wash with
273 TE buffer at RT. The DNA-protein complexes were eluted twice in 250 μl freshly
274 prepared elution buffer (0.1 M NaHCO3, 1% SDS). NaCl was added at a concentration
275 of 300 mM to the combined eluates (500 μl) before overnight incubation at 65 °C to
276 reverse the cross-link. The samples were treated with 20 μg of proteinase K in 40mM
277 EDTA and 40 mM Tris-HCl (pH 6.5) for 2 h at 45 °C. DNA was extracted using a
278 Nucleospin PCR cleanup kit (Macherey-Nagel) and resuspended in 50 μl elution buffer
279 (5 mM Tris-HCl [pH 8.5]). DNA sequencing was performed using an Illumina NextSeq
280 550 (paired-end 2x75) instrument (BIO.be). NGS data were analysed as described in
281 Coppine et al., 2020.
282
283 **RNA-seq.**
284 WT and Δ*chvI* cells were grown overnight to OD_{660} ~ 0.3 and then exposed to 6%
285 sucrose for 4 h. Thereafter, total RNA was extracted with RNeasy® Protect Bacteria
286 Kit from Qiagen and following manufacturer's instructions. The quantity and quality
287 (A260/A280 ration) of RNA was determined with a Thermo Scientific ™ Nanodrop ™
288 One Microvolume UV-Vis Spectrophotometer. RNASeq TTRNA libraries were
289 prepared according to the manufacturer's instructions and sequenced with Illumina

290 NovaSeq 6000 (paired-end 2x100) instrument (BIO.be). NGS data were analysed
291 using Galaxy (https://usegalaxy.org) (Afgan *et al.,* 2018). Briefly, FastQC was used to
292 evaluate the quality of the reads; HISAT2 was used to map the reads onto the NA1000
293 reference genome (NC_011916.1) and generate bam files; featureCounts was used
294 to generate counts tables using bam files and DESeq2 was used to determine
295 differentially expressed genes. The Volcano plot was generated using GraphPad
296 Prism 9 software.
297
298 ***In vivo* ^{32}P labelling**
299 Cells were grown overnight in PYE, then washed twice and grown in M5G medium
300 lacking phosphate and was grown overnight in M5G with 0.05 mM phosphate to OD_{660}
301 ~ 0.3. Then, one ml of culture was labelled for 4 min at 30 °C using 30 μCi γ-[^{32}P]ATP
302 (PerkinElmer). Samples were incubated with 6% sucrose, 10 μg/ml vancomycin or 100
303 μg/ml vancomycin for 7 minutes at 30 °C. Then, cells were pelleted for 2 min at 15,000
304 rpm and the supernatant removed completely without disturbing the pellets. Cell
305 pellets were resuspended in 50 μl Lysis Buffer (50 mM Tris pH 7.0, 150 mM NaCl, 80
306 mM EDTA, 2% Triton X100; sterilised with 2 μm Acrodisc syringe filters) by pipetting.
307 Lysed samples were incubated 3 min on ice, 450 μl of cold LBS were added and
308 proteins were collected using centrifugation for 15 min at 13,000 and 4 °C. Then, 40
309 μl of SureBeads Protein A Magnetic Beads (BioRad) were washed 4 times in 1 ml PBS
310 + 0.1% Tween (PBS-T) and finally resuspended in 65 μl. Thereafter, 3 μl of anti-ChvI
311 antibody were added to the washed protein A-agarose beads and incubated at RT in
312 a shaker at 1300 rpm. Protein A beads with anti-ChvI antibodies were washed 3 times
313 with PBS-T and 1 time with cold (4 °C) Low Salt Buffer (LSB; 50 mM Tris pH 7.0, 100

314 mM NaCl, 50 mM EDTA, 2% Triton X100; sterilised with 2 μm Acrodisc syringe filters),
315 immediately resuspended in 50 μl LSB and kept in ice. ChvI immunoprecipitation (IP)
316 was performed by adding the Protein A beads with anti-ChvI antibodies previously
317 prepared to the cell-free protein samples, and incubating at 4 °C with rotation for 90
318 minutes. IP samples were washed 1 time in 1 ml LSB and 3 times in 1 ml High Salt
319 Buffer (50 mM Tris pH 7.0, 500 mM NaCl, 50 mM EDTA, 0.1% Triton X100; sterilised
320 with 2 μμ Acrodisc syringe filters). Samples were eluted using 25 μl of 2.5X SDS-
321 loading Buffer and incubation at 37 °C for 5 min. Samples with SDS loading Buffer
322 were separated from magnetic beads, and 20 μl loaded on a SDS-Page gel and run
323 at 200 V-50 mA-100 W. The gel was dried for 1h at 70 °C under vacuum in a Model
324 583 Gel Dryer (BioRad). Finally, the dried gel was exposed on phosphoscreen for 5
325 days and revealed using a Cyclone Plus Phosphor Imager (PerkinElmer).
326
327 **Statistical analyses.** All the statistical analyses were performed using GraphPad
328 Prism 9 software. A *P* value of <0.05 was considered as significant.
329
330 **Data availability**
331 ChIP-Seq and RNA-Seq data have been deposited to the Gene Expression Omnibus
332 (GEO) repository with the accession number GSE200466.
333
334 ## Results
335 **High osmolyte concentration in M2G impairs growth of *chvIG* mutants**
336 It was shown previously that *C. crescentus chvIG* mutants failed to grow in minimal
337 media with xylose as sole carbon source (M2X), while these mutants grew similarly to

338 WT cells in complex media (PYE) (Stein *et al.,* 2021). Likewise, we observed that
339 mutants inoculated in M2G (with glucose as sole carbon source) in both solid and
340 liquid media were impaired for growth (**Fig. 1A-B**). To date, the cause for growth
341 impairment in *chvIG* mutants in minimal media has not been determined. Considering
342 that stressful conditions are present in synthetic minimal media (M2G or M2X) but
343 missing in PYE, we tested osmolytes as causative agents. Indeed, the synthetic
344 minimal media M2G contains a higher concentration of osmolytes than the complex
345 media PYE (Hocking *et al.,* 2012). Therefore, we assessed the viability of *chvIG*
346 mutants on plates lacking Na^+ and K^+ salts (**Fig. 1A**, M2G 0% Na^+, K^+). In these
347 conditions the *chvI* mutant grew similarly to WT cells. We also reduced these
348 osmolytes in liquid cultures, and observed that growth was restored in the *chvI* mutant
349 when half (and below) of the regular concentration found in M2G was used (**Fig. 1B**,
350 M2G 50% Na^+, K^+). Furthermore, we observed that adding osmolytes (NaCl, sucrose
351 and those in M2 salts) to complex media impaired growth and decreased viability of a
352 *chvI* mutant (**Fig. 1A**, PYEX + 40 mM NaCl, PYE + 6% Sucrose; **Fig. 1C**, PYE + M2
353 salts). Additionally, ectopic expression of *chvI* from the xylose-inducible promoter
354 (P_{xylX}*::chvI*) in a *chvI* mutant restored growth in PYEX plates supplemented with NaCl
355 whereas expressing back *chvI* in a *chvIG* mutant did not (**Fig. 1A**). Finally, while a
356 phospho-mimetic mutant of *chvI* (*chvI*$_{D52E}$) grew similarly to WT, a phospho-ablative
357 mutant of *chvI* (*chvI*$_{D52A}$) failed to propagate in M2G (**Fig. 1D**). Together, our data show
358 that a fully functional ChvGI TCS is required to survive and grow in hyperosmotic
359 environments.
360
361 **Inactivating *chvT* or *ntrX* improves fitness of a *chvI* mutant under osmotic stress**

362 Considering that mutations in *chvT* and *ntrX* partially alleviated the viability impairment
363 of *chvI* mutants in minimal media (Stein *et al*., 2021), we tested whether *chvT* or *ntrX*
364 inactivation could also partially protect *chvI* mutants from hypertonic conditions. We
365 first confirmed that a Δ*chvI* mutant was impaired for growth under osmotic stress by
366 using an excess of KCl in PYE (**Fig. 2**, PYEX + 50 mM KCl). In contrast, neither *ntrX*
367 nor *chvT* inactivation did interfere with viablity in PYE + KCl conditions compared to
368 WT (**Fig. 2**). The *ntrX* gene (previously annotated as CC1743) was suspected to be
369 essential for growth in complex PYE medium but dispensable for growth in synthetic
370 minimal medium (Skerker *et al.,* 2005). In agreement with that report, we found that
371 the viability of *ntrX* mutants was reduced in PYE (**Fig. 2**). Notwithstanding this fitness
372 cost, Δ*ntrX* Δ*chvI* double mutants could be generated and grown on PYE, as shown
373 independently in this study and by Stein *et al*. (2021). More importantly, we observed
374 that inactivating *ntrX* or *chvT* in a Δ*chvI* background partially restored growth in
375 hypertonic conditions. These data indicate that additional cell envelope defects in
376 Δ*chvI* mutants are responsible for growth impairment on hypertonic conditions.
377 Altogether, these data suggest that the homeostasis of the cell envelope is lost in
378 *chvIG* mutants, leading to a hypersensitivity to osmolytes.
379
380 **The ChvI regulon reveals osmotic stress and cell envelope-related target genes**
381 Transcriptomic analyses were previously performed on a Δ*chvI* mutant overexpressing
382 the phospho-mimetic mutant $chvI_{D52E}$ in PYE (Stein *et al.,* 2021). Nonetheless, cells
383 expressing $chvI_{D52E}$ as the only copy, either from its own promoter at the endogenous
384 *chvI* locus (P_{chvI}*::*$chvI_{D52E}$) or ectopically from the xylose-inducible promoter
385 (P_{xylX}*::*$chvI_{D52E}$) led to a slight growth delay and cell filamentation (**Fig. 1D** and **Fig.**

386 **S1**). This suggests either that $ChvI_{D52E}$ does not perfectly mimic phosphorylated ChvI
387 or that unphosphorylated ChvI is also required for optimal growth in synthetic minimal
388 media. Hence, we determined the ChvI regulon of WT cells grown in M2G by using
389 ChIP-seq with polyclonal antibodies targeting ChvI, which allowed to unveil the DNA
390 regions directly bound by ChvI (**Fig. 3A**, **Table S4**).
391 From our experiment, 190 peaks (DNA binding sites) were identified for ChvI (**Fig. 3A**,
392 **Table S4**). Interestingly, the top target is the promoter region of *chvT* itself, suggesting
393 that ChvI regulates ChvT not only (i) indirectly at the post-transcriptional level via
394 transcriptional activation of the sRNA *chvR* but also (ii) directly at the transcriptional
395 level and (**Fig. 3A**). Besides *chvT* and *chvR*, we identified potential new targeted
396 genes involved in (i) cell division, morphology and peptidoglycan (PG) synthesis, such
397 as *mreB*, *ftsZ*, *ftsN* and *dipM*; and (ii) general stress response (GSR), such as *sigT*
398 (sigma factor T), *nepR* (*sigT* antagonist) and *phyKR* (TCS regulating NepR activity
399 negatively).
400 To further confirm some of the new targeted genes, we tested their expression by
401 measuring their promoter activity upon osmotic shock. As shown in **Fig. 3B**, the activity
402 of *dipM* and *ftsN* promoters was significantly lower in the Δ*chvI* mutant compared to
403 WT, whereas *phyR* promoter activity was significantly higher in Δ*chvI* than in WT. In
404 contrast, the *nepR* promoter had similar activity in both WT and Δ*chvI* strains. These
405 results suggest that ChvI can work as an activator (e.g. *dipM* and *ftsN*) or a repressor
406 (e.g. *phyR*) of gene expression.
407 Interestingly, *hprK* is part of the SigT regulon determined upon osmotic shock (Tien *et*
408 *al.*, 2018). Given that *hprK* is part of the same operon as *chvIG*, we tested whether the
409 entire operon *chvIG-hprK* could be under the control of SigT. Consistently, we found

410 that in cells grown in PYE, washed and exposed for four hours in M2G, the *chvI*
411 promoter (P_{chvI}) was significantly higher in the Δ*sigT* mutant compared to WT whereas
412 the activity of P_{chvI} was strongly reduced in the Δ*chvI* mutant (**Fig. S2A**). Thus, SigT is
413 a negative regulator of ChvI while ChvI is subjected to a positive feedback loop.
414 Considering that *phyR* promoter activity was higher in a Δ*chvI* background **(Fig. 3B**),
415 this indicates that ChvI regulates negatively SigT by inhibiting PhyR. To better
416 understand the regulatory mechanism between ChvI and SigT we tested viability of
417 mutants for the genes in osmotic conditions used in this study, that is PYE
418 supplemented 40 mM NaCl (**Fig. 1A**), but also in more stringent conditions used in a
419 previous study, that is PYE supplemented 85 mM NaCl (Alvarez-Martinez *et al.,* 2007)
420 (**Fig. S2B**). We observed that, contrary to *chvI*, *sigT* is not essential for viability in PYE
421 + 40 mM NaCl. In contrast, at a higher osmotic regime (PYE + 85m M NaCl) the
422 viability of Δ*sigT* declined. Moreover, inactivating *sigT* in a Δ*chvI* background did not
423 aggravate the poor viability of Δ*chvI* mutant upon osmotic stress. Together, these data
424 suggest that ChvGI responds to lower osmotic stress than SigT and that both SigT
425 and ChvI antagonise each other at the transcriptional level.
426 We also performed RNA-seq on WT and Δ*chvI* cells grown in PYE and exposed to 6%
427 sucrose for 4 hours. We found 301 down-regulated and 293 up-regulated genes with
428 ≥1.5-fold change and a false-discovery rate [FDR] $P_{adj} \leq 0.05$ (**Fig. 3C**; **Tables S5**
429 and **S6**). Among these genes, 126 down-regulated and 44 up-regulated genes were
430 identified in our ChIP-seq experiment (**Tables S5** and **S6**). This further suggests that
431 ChvI performs direct dual positive and negative transcriptional regulation, but mostly
432 positive. Furthermore, we confirmed that upon osmotic shock, ChvI regulates the
433 expression of multiple genes involved in cell envelope homeostasis such as for

434 example, *tol* genes, *bam* genes and TBDR-encoding genes (**Fig. 3C**; **Tables S5** and
435 **S6**).

436 **ChvI is phosphorylated under osmotic upshift**

437 Since both single Δ*chvG* and Δ*chvI* mutants are sensitive to osmotic upshift (**Fig. 1A**),
438 this suggests that ChvI might be phosphorylated and activated by ChvG in such
439 stressful conditions. We tested this hypothesis by determining the *in vivo*
440 phosphorylated levels of ChvI (ChvI~P) with or without osmotic shock. In order to
441 facilitate uptake of [γ-^{32}P] ATP, *Caulobacter* cells were grown in a medium depleted
442 for the phosphate salts Na_2HPO_4 and KH_2HPO_4 (M5GG). Hence, K^+ and Na^+
443 concentrations in M5GG are respectively 1.01 mM and 1.02 mM, which is much less
444 that in M2G (7.75 mM of K^+ and 12.25 mM of Na^+). At such low concentrations of
445 osmolytes, the Δ*chvI* strain grew, as expected, similarly to WT in M5GG (**Fig. 4A**). In
446 contrast and in agreement with our previous findings, the growth of the Δ*chvI* mutant
447 was severely impaired in M5GG supplemented with 6% sucrose compared to WT (**Fig.**
448 **4A**). Consistent with these data, we observed that ChvI was barely phosphorylated in
449 WT grown in M5GG while no ChvI~P was detected in Δ*chvG* (**Fig. 4B**). More
450 importantly, ChvI was hyperphosphorylated in cells grown under osmotic shock with
451 sucrose (**Fig. 4C-D**).

452

453 **ChvGI is sensitive to peptidoglycan synthesis inhibition**

454 Stress response systems surveying cell envelope homeostasis in Gram-negative
455 bacteria are sensitive to different stressful conditions including osmotic shock (Jubelin
456 *et al.,* 2005; Laubacher & Ades, 2008; Cho *et al.,* 2014). Moreover, deletion of the
457 *chvGI-hprK* operon have been shown to result in sensitivity to vancomycin (Vallet *et*

458 *al.,* 2020), which targets the D-Ala-D-Ala moiety of the PG precursors thereby
459 inhibiting PG crosslinking. First, we confirmed that vancomycin impairs growth and
460 viability of the single Δ*chvI* mutant (**Fig 5.A** and **E**). We also tested growth and viability
461 upon treatment with other cell envelope stressors, such as acidic pH, detergent and
462 antibiotics targeting the outer membrane or the PG synthesis machinery. We did not
463 observe significant impacts on fitness between WT and Δ*chvI* cells under treatment
464 with acidic stress, A22 drug targeting the actin-like protein MreB, SDS and polymyxin
465 B which target the outer membrane, and the antibiotic cephalexin, which inhibits the
466 PG transpeptidase activity of the Penicillin Binding Protein 3 (Pbp3) associated to the
467 cell division machinery (divisome) (**Fig. S3A-B**). In contrast, we found that exposure
468 to other antibiotics targeting PBPs associated to cell elongation machinery
469 (elongasome) impaired growth of the Δ*chvI* mutant. For instance, treatment with
470 mecillinam, which inhibits PG crosslinking during elongation by binding to Pbp2
471 significantly impaired growth and viability of Δ*chvI* cells compared to WT (**Fig. 5B** and
472 **E**). Also, treatment with antibiotics targeting the bifunctional
473 glycosyltranferase/transpeptidase Pbp1a, such as Cefsulodin and Moenomycin also
474 diminished the growth and viability of the Δ*chvI* mutant (**Fig. 5B-C** and **E**). Altogether,
475 these results indicated that ChvGI is a TCS responding to osmotic upshift but also to
476 PG crosslinking damage.
477 To confirm this, similar to cell exposed with osmotic stress, we assessed the
478 phosphorylation of ChvI following exposure to vancomycin or mecillinam antibiotics
479 (**Fig. 5F**). We observed that ChvI phosphorylation increased after vancomycin but not
480 mecillinam treatment. To better understand this result, and considering that the *chvIG-*
481 *hprK* operon is under positive autoregulation by ChvI~P, we assessed the activity of

482 the P_{chvI}*::lacZ* transcriptional reporter in synthetic media M5GG supplemented with
483 vancomycin or mecillinam (**Fig. 5G**). We observed that activity of the *chvI* promoter
484 significantly increased after exposure to both antibiotics but the response was faster
485 with vancomycin (1 hr) than with mecillinam (3 hrs) treatment. Surprisingly, although
486 the activity of P_{chvI}*::lacZ* was lower in Δ*chvI* cells than in WT cells, it remained higher
487 in Δ*chvI* treated cells than in Δ*chvI* untreated cells, even though this difference was
488 significant only for mecillinam (**Fig. 5G**). Together, these data suggest that (i) the
489 response to mecillinam treatment is slower than the one to vancomycin and that (ii)
490 *chvIG-hprK* expression following exposure to antibiotics is induced not only by ChvI
491 itself but also in a ChvI-independent way.
492
493 **ChvG relocates from patchy-spotty to midcell upon osmotic shock**
494 Intriguingly, the HK ChvG was previously found in an automated large-scale analysis
495 for protein localisation as displaying a patchy-spotty distribution typically observed with
496 PG-related proteins (Werner *et al.,* 2009). Therefore, we constructed fluorescent
497 protein fusions to analyse ChvG and ChvI localisation patterns on PYE and M2G pads.
498 First, we confirmed that GFP fusions to the N- or C-terminal extremity of ChvG or ChvI
499 were stable and functional, as attested by western blot analyses and growth assays
500 (**Fig. S4AB**). Then, fluorescent microscopy images showed that both ChvG N- and C-
501 terminal fusions to GFP displayed patchy-spotty localisation patterns in cells grown in
502 PYE or M2G cultures (**Fig. 6A**, **Fig. S4C**). We also confirmed the patchy-spotty
503 localisation pattern for the ChvG C-terminal fusion to GFP in high resolution confocal
504 microscopy (**Fig. S4D**). Surprisingly, when cells grown in PYE were washed in M2G
505 and imaged on M2G agar pads, we observed some cells formed foci near mid-cell

506 (**Fig. 6A**). In contrast, cells grown in M2G, washed with PYE and imaged on PYE pad
507 kept their patchy-spotty localisation pattern (**Fig. 6A**). This relocation is reminiscent to
508 what was described for the PG-related proteins RodA, PBP2 and PBP1A, whose
509 localization changed from a typical patchy-spotty distribution to mid-cell when cells
510 were shifted from PYE to M2G agarose pads (Hocking *et al.,* 2012).
511 In contrast to ChvG, none of the ChvI fusions to GFP (ChvI-GFP and GFP-ChvI)
512 displayed patchy-spotty localization nor foci formation was detected after transition
513 from PYE to M2G pads (**Fig. 6B** and data not shown). Instead, the signal was diffused
514 all over the cell body, indicating that the protein remains diffused in the cytoplasm.
515 Then, we wanted to assess if the catalytic activity had any impact on the protein
516 localisation. For that, we fused GFP to a full-length catalytic mutant of ChvG to
517 ($ChvG_{H309N}$), which like Δ*chvG* was unable to grow on M2G (**Fig. S4E-F**). We observed
518 that, similar to the WT ChvG-GFP, the $ChvG_{H309N}$-GFP showed a patchy-spotty
519 pattern when cells were grown in PYE and relocated at mid-cell when shifted from
520 PYE to M2G (**Fig. 6C**). Thus, our data suggest that ChvG co-localizes with PG
521 synthesis machinery independently of its kinase activity.
522
523 **The N-terminal extremity of ChvG determines localisation and relocation**
524 ChvG is a HK anchored in the membrane thanks to 2 transmembrane helices which
525 delimit a periplasmic sensor domain (amino acids 50-221), with a cytoplasmic signal
526 transduction histidine kinase domain (amino acids 242-534) (**Fig. 7A**). To assess
527 which of these ChvG domains are essential for localisation, we fused to mCherry
528 ChvG versions harbouring either the complete ($ChvG_{1-274}$ and $ChvG_{1-202}$) or truncated
529 sensor ($ChvG_{1-114}$) or the catalytic ($ChvG_{273-534}$) domain. First, we showed that both

530 sensor and catalytic domains are essential for *C. crescentus* to propagate in high
531 osmolytes conditions like in M2G since mutants harbouring in frame deletion of each
532 of these domains ($ChvG_{274-534}$ or $ChvG_{1-274}$) were unable to survive in M2G (**Fig. S4G**).
533 Then, we observed that full-length ChvG fused to mCherry displayed similar
534 localisation and relocation patterns (**Fig. 7B-C**) than the ones described for GFP
535 fusions (**Fig. 6A**). Interestingly, the truncated or complete sensor domain alone
536 ($ChvG_{1-114}$, $ChvG_{1-202}$, $ChvG_{1-274}$) fused to mCherry were both localized as patchy-
537 spotty in PYE (**Fig. 7B**). However, only the full-length ChvG-mCherry and $ChvG_{1-274}$-
538 mCherry fusions relocated as foci upon transition to M2G, even though $ChvG_{1-274}$-
539 mCherry foci were not often found at midcell (**Fig. 7C**). Unlike the sensor domain
540 truncates, the catalytic domain ($ChvG_{273-534}$) fused to mCherry displayed neither the
541 patchy-spotty nor the foci pattern of localization and was instead diffusely localized in
542 the cytoplasm (**Fig. 7**B-C). Altogether, our results indicate that the complete
543 periplasmic sensor domain of ChvG edged by transmembrane domains are required
544 for relocation as foci upon osmotic shock whereas the first 114 amino acids are
545 sufficient to determine the patchy-spotty pattern of localization.
546

547 ## Discussion

548 The α-proteobacterial TCS ChvGI has conserved cell envelope regulatory functions
549 (Lamontagne *et al*., 2007; Heckel *et* al., 2014; Ratib *et al*., 2018; Vallet *et al*., 2020;
550 Stein *et al*., 2021), but the exact perceived signals that trigger the ChvG-dependent
551 phosphorylation of ChvI remained unknown. We found that hyperosmotic shock and
552 antibiotic treatment harming PG crosslinking stimulates ChvI phosphorylation. Also,
553 we showed that other antibiotics targeting PG synthesis proteins induce *chvIG*
554 expression and impair fitness of the Δ*chvI* mutant. On top of this, we showed that ChvI
555 regulates expression of genes related to PG synthesis, such as *ftsN* and *dipM*, and to
556 osmotic and oxidative stress regulation, such as *nepR*, likely explaining why ChvGI
557 system is required for viability in these stressful conditions. Other targets related to
558 cell envelope architecture, identified by ChIP-seq and RNA-seq experiments, include
559 genes coding for the β-barrel assembly machinery (Bam) complex; components of the
560 Tol system; several outer membrane proteins (OMP) such as RasFa, CCNA_03820
561 and CCNA_01956, and several TBDR proteins; and the cytoplasmic FtsZ-binding
562 protein ZapA. Altogether, our results support a role for ChvGI in *C. crescentus* as a
563 safeguard of cell envelope homeostasis by sensing cell wall-related damages and
564 regulating the expression of genes related to cell division and envelope architecture.
565 In the absence of a functional ChvGI system, *C. crescentus* cannot propagate in
566 minimal media except if the TonB-dependent outer membrane protein ChvT or if NtrX
567 is concomitantly inactivated (Stein *et al.,* 2021). ChvGI is known to indirectly down-
568 regulate ChvT by directly activating the expression of the sRNA ChvR (Fröhlich *et al*.,
569 2018). Our ChIP-seq data showed that ChvI also likely regulates *chvT* expression
570 directly by binding to its promoter region. This dual – transcriptional and post-

571 transcriptional – control indicates the ChvT outer membrane protein is an important
572 player in cell envelope homeostasis. Interestingly, NtrYX has been also described as
573 a cell envelope regulator in α-proteobacteria. NtrYX controls succinoglycan and
574 exopolysaccharide (EPS) production, and salt stress response in *S. meliloti* (Wang *et*
575 *al*., 2013; Calatrava *et al*., 2017). In *Rhodobacter sphaeroides,* NtrYX confers
576 resistance to membrane disruptive agents and regulates the expression of genes
577 coding for PG and EPS synthesis enzymes, lipoproteins and cell division proteins
578 (Lemmer *et al.,* 2017; Lemmer *et al*., 2020). Thus, confirming that *ntrX* inactivation in
579 a Δ*chvI* background partially restored growth in the presence of high concentration of
580 osmolytes further supports the importance of the NtrZXY system, together with ChvGI,
581 in the cell envelope stress response in α-proteobacteria.
582 In *C. crescentus*, the general stress response (GSR) sigma factor SigT is also
583 activated upon osmotic imbalance thanks to a complex network comprising the sRNA
584 (GsrN), the anti-SigT regulator (NepR), the histidine phosphotransferases (LovK and
585 PhyK) and the RR (MrrA, LovR and PhyR) (Alvarez-Martinez *et al*., 2007; Lourenço *et*
586 *al*., 2011; Foreman *et al*., 2012; Lori *et al*., 2018; Tien *et al*., 2018). In steady-state
587 conditions, NepR impedes SigT-dependent transcription. Upon either oxidative stress
588 or osmotic imbalance, the histidine phosphotransferase MrrA activates PhyK to further
589 phosphorylate PhyR. Once phosphorylated, PhyR~P interacts with NepR to release
590 SigT from inhibition and allow the expression the SigT-dependent regulon.
591 Interestingly, we found that ChvGI and GSR are interconnected but this connection is
592 counterintuitive. Indeed, we observed (i) that deletion of *sigT* led to higher *chvI*
593 promoter activity and (ii) that ChvI directly represses *phyR* expression, suggesting that
594 ChvI and SigT antagonise each other while being sensitive to hyperosmotic

595 conditions. However, we cannot exclude the possibility that the cell envelope
596 homeostasis is sufficiently disrupted in both single mutants to correspondingly activate
597 the other functional system, *i.e.* ChvGI in Δ*sigT* through P_{chvIG} and SigT in Δ*chvI*
598 through P_{phyR}. The antagonistic regulation might allow the response of the systems to
599 different levels of osmotic imbalances. For instance, activation of ChvGI at low
600 hypertonic conditions could down-regulate GSR whereas SigT would be sensitive to
601 higher salts concentrations to which ChvGI is turned down. In agreement with this
602 hypothesis, we found that SigT is essential in more severe osmotic scenarios
603 compared to ChvI.
604 In addition, constitutive activation of a cell envelope stress response system can be
605 detrimental. Overexpression of a phosphomimetic *chvI* variant has been shown to
606 complement growth, but also to result in dysfunctional filamentous growth in minimal
607 media (Stein *et al.,* 2021). The importance of negative regulation of cell envelope
608 stress response systems has been lucidly demonstrated in *E. coli* with the sigma factor
609 E (σ^E), the inner membrane stress regulator Cpx or the regulator of capsule synthesis
610 Rcs (Missiakas *et al.*, 1997; Pogliano *et al.*, 1998; De Las Peñas *et al.*, 2003;
611 Grabowicz & Silhavy. 2017), Indeed, overactivation of σ^E causes overexpression of
612 sRNAs inhibiting expression of integral OMPs, therefore weakening the outer
613 membrane integrity (Nicoloff *et al.*, 2017). Likewise, constitutive Cpx activation
614 disturbs cell division and morphology causing mis-localisation of FtsZ as well as
615 overexpression of L,D-transpeptidase enzyme LdtD (Pogliano *et al.*, 1998; Delhaye *et*
616 *al.,* 2016). Similarly, overactivation of the RR RcsB results in overexpression of the
617 small outer membrane lipoprotein OsmB, which is toxic through yet unknown

618 mechanisms (Grabowicz & Silhavy. 2017). In any of the previous cases,
619 hyperstimulation can lead to deregulation of cell envelope components.
620 We showed that ChvGI also regulates sensitivity to the antibiotic mecillinam,
621 cefsulodin and moenomycin which inhibit PG transpeptidation. Previously, Vallet *et al.*
622 (2020) showed a mutant for the *chvIG-hprk* operon failed to grow when exposed to
623 vancomycin, which also impedes PG crosslinking by directly interacting with the D-
624 Ala-D-Ala moiety of the PG precursors. Here, we showed that ChvI was
625 phosphorylated when exposed to vancomycin but not to mecillinam. However,
626 although both antibiotics inhibit the transpeptidation step of PG synthesis, they
627 induced *chvIG* expression in different time windows. In addition, these antibiotics cross
628 the outer membrane with different efficiency. For instance, vancomycin is likely
629 efficiently transported by the TBDR ChvT, thereby reaching high concentration in the
630 periplasm in minutes. It is therefore possible that ChvGI is systematically activated
631 upon inhibition of PG transpeptidation during cell elongation but with different
632 sensitivity depending on the transport rate for each antibiotic.
633 In contrast to the stressors mentioned above, treatment with cefixime, cefotaxime and
634 sodium deoxycholate did not show differences in cell viability between WT and
635 Δ*chvIG-hprk* cells (Vallet *et al.*, 2020). Furthermore, the activation of *chvR* expression
636 upon cefotaxime or sodium deoxycholate exposure was shown to be ChvI-
637 independent. In addition, we showed here that Δ*chvI* cells were not more sensitive to
638 treatment with SDS, polymyxin B or the MreB inhibitor A22. Considering that MreB is
639 a key cytoplasmic component of the elongasome complex, of which PBP2 and other
640 proteins are part, it is therefore likely that ChvGI rather senses specific targets in the
641 periplasm to assess cell envelope stress. We propose that ChvG phosphorylation is

642 stimulated by hyperosmotic conditions or antibiotics targeting PG transpeptidation by
643 specifically sensing the pressure or the integrity of the peptidic crosslinks of PG
644 instead of glycan strands. In such a scenario, the periplasmic sensor domain of ChvG
645 could interact with components of the elongasome or bind peptide bridges of the PG.
646 Notwithstanding that, other stress response systems, yet to be discovered or
647 characterised in the context of the aforementioned stressors, might be involved in
648 responding to the damages that do not activate ChvGI.
649 We observed that ChvG has a patchy-spotty localisation pattern when grown in
650 complex and synthetic minimal media, while it relocates as foci near mid-cell upon
651 transition from complex to minimal media. The patchy-spotty localisation pattern has
652 been described for multiple PG-related proteins in *C. crescentus*, including MreB,
653 MreC, Pal, PBP1A, PBP2, RodA, TolB (Figge *et* al., 2004; Divakaruni *et al.,* 2005;
654 Werner *et al*., 2009; Hocking *et al.,* 2012; Billini *et al*., 2019). Moreover, RodA, PBP2,
655 PBP1A, which are proteins involved in PG polymerization and crosslinking, have been
656 reported to relocate at mid-cell upon osmotic upshift in a FtsZ-dependent but MreB-
657 independent manner (Hocking *et al.,* 2012). It would be interesting to check whether
658 this ChvG localisation patterns are conserved among α-proteobacteria, in particular in
659 Rhizobiales since they do not encode MreB orthologs. In *E. coli*, it has been reported
660 that the PBP2 periplasmic portion physically interacts with those of PBP1A and RodA
661 to mediate PG assembly and to ensure proper cell elongation (Banzhaf *et al*., 2012;
662 van der Ploeg *et al*., 2015). It is yet to determine whether ChvG interacts with PBP2,
663 PBP1a, RodA and/or others with similar localisation patterns. Nonetheless, it is
664 tempting to speculate that ChvG interacts and co-localises with PG-related enzymes
665 as a cell envelope safeguard system in α-proteobacteria. A recent study in the Gram-

666 positive bacterium *Bacillus thuringiensis* showed that upon treatment with the
667 antibiotic cefoxitin, the putative PBP protein PbpP derepresses the extracytoplasmic
668 function sigma factor P (σ^P) which increases resistance to β-lactams (Nauta *et al.*,
669 2021). Future experiments will aim to determine the ChvG interactome under cell
670 envelope undisturbed and threatening conditions, and dissect its activation
671 mechanism as well as its connection with the general stress response, not only in *C.*
672 *crescentus* but also in other α-proteobacteria.
673

674 **Acknowledgments**

675 We are grateful to Clare Kirkpatrick, Sean Crosson and Benjamin Stein for willingness
676 to discuss and share data on their ChvGI-related projects. Also, we would like to thank
677 members of the URBM of the University of Namur for their comments and suggestions
678 on this project, especially Dr. Angéline Reboul for her comments and advices on the
679 microscopy analysis, Jérôme Coppine for constructing some strains and members of
680 the Hallez lab for their comments on the manuscript. This work was supported by the
681 Fonds de la Recherche Scientifique – FNRS (F.R.S. – FNRS) with a Welbio Starting
682 Grant (WELBIO-CR-2019S-05) to R.H. A.Q-Y. was supported by a postdoctoral
683 fellowship from the University of Namur (UNamur). R.H. is a Research Associate of
684 F.R.S. – FNRS.
685

686 **Author Contributions**

687 A.Q-Y. and R.H. conceived and designed the experiments. A.Q-Y. performed all the
688 experiments except otherwise stated. A.M. purified the ChvI protein and helped with

689 some plasmid's constructs. A.Q-Y. and R.H. analyzed the data. A.Q-Y. and R.H. wrote

690 the paper.

691

692 **Competing financial interests**

693 The authors declare no competing financial interests.

694

695 **References**

696 Afgan, E., Baker, D., Batut, B., Van Den Beek, M., Bouvier, D., Čech, M., ... &
697 Blankenberg, D. (2018). The Galaxy platform for accessible, reproducible and
698 collaborative biomedical analyses: 2018 update. *Nucleic acids research*, *46*(W1),
699 W537-W544.

700

701 Altamirano-Silva, P., Meza-Torres, J., Castillo-Zeledón, A., Ruiz-Villalobos, N.,
702 Zuñiga-Pereira, A. M., Chacón-Díaz, C., … & Chaves-Olarte, E. (2018). *Brucella*
703 *abortus* senses the intracellular environment through the BvrR/BvrS two-component
704 system, which allows *B. abortus* to adapt to its replicative niche. *Infection and*
705 *immunity*, *86*(4), e00713-17.

706

707 Alvarez-Martinez, C. E., Lourenço, R. F., Baldini, R. L., Laub, M. T., & Gomes, S. L.
708 (2007). The ECF sigma factor σT is involved in osmotic and oxidative stress responses
709 in *Caulobacter crescentus*. *Molecular microbiology*, *66*(5), 1240-1255.

710

711 Banzhaf, M., van den Berg van Saparoea, B., Terrak, M., Fraipont, C., Egan, A.,
712 Philippe, J., ... & Vollmer, W. (2012). Cooperativity of peptidoglycan synthases active
713 in bacterial cell elongation. *Molecular microbiology*, *85*(1), 179-194.

714

715 Beaufay F., Coppine J., Mayard A., Laloux G., De Bolle X. & Hallez R. (2015). A NAD-
716 dependent glutamate dehydrogenase coordinates metabolism with cell division in
717 *Caulobacter crescentus*. *The EMBO Journal*, *34*(13), 1786-800

718

719 Billini, M., Biboy, J., Kühn, J., Vollmer, W., & Thanbichler, M. (2019). A specialized
720 MreB-dependent cell wall biosynthetic complex mediates the formation of stalk-
721 specific peptidoglycan in *Caulobacter crescentus*. *PLoS genetics*, *15*(2), e1007897.
722
723 Calatrava-Morales, N., Nogales, J., Ameztoy, K., van Steenbergen, B., & Soto, M. J.
724 (2017). The NtrY/NtrX system of *Sinorhizobium meliloti* GR4 regulates motility, EPS I
725 production, and nitrogen metabolism but is dispensable for symbiotic nitrogen
726 fixation. *Molecular Plant-Microbe Interactions*, *30*(7), 566-577.
727
728 Capra, E. J., & Laub, M. T. (2012). Evolution of two-component signal transduction
729 systems. *Annual review of microbiology*, *66*, 325-347.
730
731 Carrica, M. D. C., Fernandez, I., Martí, M. A., Paris, G., & Goldbaum, F. A. (2012).
732 The NtrY/X two-component system of *Brucella* spp. acts as a redox sensor and
733 regulates the expression of nitrogen respiration enzymes. *Molecular*
734 *microbiology*, *85*(1), 39-50.
735
736 Chen, E. J., Sabio, E. A., & Long, S. R. (2008). The periplasmic regulator ExoR inhibits
737 ExoS/ChvI two-component signalling in *Sinorhizobium meliloti*. *Molecular*
738 *microbiology*, *69*(5), 1290-1303.
739
740 Cho, S. H., Szewczyk, J., Pesavento, C., Zietek, M., Banzhaf, M., Roszczenko, P., ...
741 & Collet, J. F. (2014). Detecting envelope stress by monitoring β-barrel
742 assembly. *Cell*, *159*(7), 1652-1664.

743

744 Coppine J., Kaczmarczyk A., Petit K., Brochier T., Jenal U. & Hallez R. (2020).
745 Regulation of bacterial cell cycle progression by redundant phosphatases. *Journal of*
746 *bacteriology*, *202*(17), e00345-20

747

748 De Las Peñas, A., Connolly, L., & Gross, C. A. (1997). The σE-mediated response to
749 extracytoplasmic stress in *Escherichia coli* is transduced by RseA and RseB, two
750 negative regulators of σ^E. *Molecular microbiology*, *24*(2), 373-385.

751

752 Delhaye, A., Collet, J. F., & Laloux, G. (2016). Fine-tuning of the Cpx envelope stress
753 response is required for cell wall homeostasis *in Escherichia coli*. *MBio*, *7*(1), e00047-
754 16.

755

756 Divakaruni, A. V., Loo, R. R. O., Xie, Y., Loo, J. A., & Gober, J. W. (2005). The cell-
757 shape protein MreC interacts with extracytoplasmic proteins including cell wall
758 assembly complexes in *Caulobacter crescentus*. *Proceedings of the National*
759 *Academy of Sciences*, *102*(51), 18602-18607.

760

761 Ducret, A., Quardokus, E. M., & Brun, Y. V. (2016). MicrobeJ, a tool for high throughput
762 bacterial cell detection and quantitative analysis. *Nature Microbioly* 1: 16077.

763

764 Ely, B. (1991). [17] Genetics of *Caulobacter crescentus*. *Methods in enzymology*, *204*,
765 372-384.

766

767 Figge, R. M., Divakaruni, A. V., & Gober, J. W. (2004). MreB, the cell shape-
768 determining bacterial actin homologue, co-ordinates cell wall morphogenesis in
769 *Caulobacter crescentus*. *Molecular microbiology*, *51*(5), 1321-1332.
770
771 Foreman, R., Fiebig, A., & Crosson, S. (2012). The LovK-LovR two-component system
772 is a regulator of the general stress pathway in *Caulobacter crescentus*. *Journal of*
773 *bacteriology*, *194*(12), 3038-3049.
774
775 Fröhlich, K., Förstner, K., & Gitai, Z. Post-transcriptional gene regulation by an Hfq-
776 independent small RNA in *Caulobacter crescentus*. *Nucleic acids research*, *46*(20),
777 10969-10982
778
779 Gao, R., & Stock, A. M. (2009). Biological insights from structures of two-component
780 proteins. *Annual review of microbiology*, *63*, 133-154
781
782 Goulian, M. (2010). Two-component signaling circuit structure and properties. *Current*
783 *opinion in microbiology*, *13*(2), 184-189.
784
785 Grabowicz, M., & Silhavy, T. J. (2017). Redefining the essential trafficking pathway for
786 outer membrane lipoproteins. *Proceedings of the National Academy of*
787 *Sciences*, *114*(18), 4769-4774
788
789 Heckel, B. C., Tomlinson, A. D., Morton, E. R., Choi, J. H., & Fuqua, C. (2014).
790 *Agrobacterium tumefaciens exoR* controls acid response genes and impacts

791 exopolysaccharide synthesis, horizontal gene transfer, and virulence gene
792 expression. *Journal of bacteriology*, *196*(18), 3221-3233.
793
794 Hocking, J., Priyadarshini, R., Takacs, C. N., Costa, T., Dye, N. A., Shapiro, L., ... &
795 Jacobs-Wagner, C. (2012). Osmolality-dependent relocation of penicillin-binding
796 protein PBP2 to the division site in *Caulobacter crescentus*. *Journal of*
797 *bacteriology*, *194*(12), 3116-3127.
798
799 Jubelin, G., Vianney, A., Beloin, C., Ghigo, J. M., Lazzaroni, J. C., Lejeune, P., & Dorel,
800 C. (2005). CpxR/OmpR interplay regulates curli gene expression in response to
801 osmolarity in *Escherichia coli. Journal of bacteriology*, *187*(6), 2038-2049.
802
803 Lamontagne, J., Butler, H., Chaves-Olarte, E., Hunter, J., Schirm, M., Paquet, C., ...
804 & Paramithiotis, E. (2007). Extensive cell envelope modulation is associated with
805 virulence in *Brucella abortus*. *Journal of proteome research*, *6*(4), 1519-1529.
806
807 Laubacher, M. E., & Ades, S. E. (2008). The Rcs phosphorelay is a cell envelope
808 stress response activated by peptidoglycan stress and contributes to intrinsic antibiotic
809 resistance. *Journal of bacteriology*, *190*(6), 2065-2074.
810
811 Lemmer, K. C., Alberge, F., Myers, K. S., Dohnalkova, A. C., Schaub, R. E., Lenz, J.
812 D., ... & Donohue, T. J. (2020). The NtrYX two-component system regulates the
813 bacterial cell envelope. *Mbio*, *11*(3), e00957-20.
814

815 Lemmer, K. C., Zhang, W., Langer, S. J., Dohnalkova, A. C., Hu, D., Lemke, R. A., ...
816 & Donohue, T. J. (2017). Mutations that alter the bacterial cell envelope increase lipid
817 production. *Mbio*, *8*(3), e00513-17.
818
819 Li, L., Jia, Y., Hou, Q., Charles, T. C., Nester, E. W., & Pan, S. Q. (2002). A global pH
820 sensor: *Agrobacterium* sensor protein ChvG regulates acid-inducible genes on its two
821 chromosomes and Ti plasmid. *Proceedings of the National Academy of*
822 *Sciences*, *99*(19), 12369-12374.
823
824 Lori, C., Kaczmarczyk, A., de Jong, I., & Jenal, U. (2018). A single-domain response
825 regulator functions as an integrating hub to coordinate general stress response and
826 development in Alphaproteobacteria. *MBio*, *9*(3), e00809-18.
827
828 Lourenço, R. F., Kohler, C., & Gomes, S. L. (2011). A two-component system, an anti-
829 sigma factor and two paralogous ECF sigma factors are involved in the control of
830 general stress response in *Caulobacter crescentus*. *Molecular microbiology*, *80*(6),
831 1598-1612.
832
833 Mantis, N. J., & Winans, S. C. (1993). The chromosomal response regulatory gene
834 chvI of *Agrobacterium tumefaciens* complements an *Escherichia coli phoB* mutation
835 and is required for virulence. *Journal of bacteriology*, *175*(20), 6626-6636.
836

837 Missiakas, D., Mayer, M. P., Lemaire, M., Georgopoulos, C., & Raina, S. (1997).
838 Modulation of the *Escherichia coli* σ^E (RpoE) heat-shock transcription-factor activity
839 by the RseA, RseB and RseC proteins. *Molecular microbiology*, *24*(2), 355-371.
840
841 Nauta, K. M., Ho, T. D., & Ellermeier, C. D. (2021). The Penicillin-Binding Protein PbpP
842 Is a Sensor of β-Lactams and Is Required for Activation of the Extracytoplasmic
843 Function σ Factor σ^P in *Bacillus thuringiensis*. *Mbio*, *12*(2), e00179-21.
844
845 Nicoloff, H., Gopalkrishnan, S., & Ades, S. E. (2017). Appropriate regulation of the σ^E-
846 dependent envelope stress response is necessary to maintain cell envelope integrity
847 and stationary-phase survival in *Escherichia coli. Journal of bacteriology*, *199*(12),
848 e00089-17.
849
850 Pawlowski, K., Klosse, U., & De Bruijn, F. J. (1991). Characterization of a novel
851 *Azorhizobium caulinodans* ORS571 two-component regulatory system, NtrY/NtrX,
852 involved in nitrogen fixation and metabolism. *Molecular and General Genetics*
853 *MGG*, *231*(1), 124-138.
854
855 Pogliano, J., Dong, J. M., De Wulf, P., Furlong, D., Boyd, D., Losick, R., ... & Lin, E.
856 C. C. (1998). Aberrant cell division and random FtsZ ring positioning in *Escherichia*
857 *coli cpxA** mutants. *Journal of bacteriology*, *180*(13), 3486-3490.
858
859 Ratib, N. R., Sabio, E. Y., Mendoza, C., Barnett, M. J., Clover, S. B., Ortega, J. A., ...
860 & Chen, E. J. (2018). Genome-wide identification of genes directly regulated by ChvI

and a consensus sequence for ChvI binding in *Sinorhizobium meliloti*. *Molecular microbiology*, *110*(4), 596-615.

Ronneau S., Petit K., De Bolle X., Hallez R. (2016). Phosphotransferase-dependent accumulation of (p)ppGpp in response to glutamine deprivation in *Caulobacter crescentus*. *Nature Communications*, 7, 11423.

Skerker, J. M., Prasol, M. S., Perchuk, B. S., Biondi, E. G., & Laub, M. T. (2005). Two-component signal transduction pathways regulating growth and cell cycle progression in a bacterium: a system-level analysis. *PLoS biology*, *3*(10), e334

Stein, B. J., Fiebig, A., & Crosson, S. (2021). The ChvG–ChvI and NtrY–NtrX two-component systems coordinately regulate growth of *Caulobacter crescentus*. *Journal of Bacteriology*, JB-00199.

Stock, A. M., Robinson, V. L., & Goudreau, P. N. (2000). Two-component signal transduction. *Annual review of biochemistry*, *69*(1), 183-215.

Tien, M. Z., Stein, B. J., & Crosson, S. (2018). Coherent feedforward regulation of gene expression by *Caulobacter* σ^T and GsrN during hyperosmotic stress. *Journal of bacteriology*, *200*(19), e00349-18.

885 Vallet, S. U., Hansen, L. H., Bistrup, F. C., Laursen, S. A., Chapalay, J. B., Chambon,
886 M., ... & Kirkpatrick, C. L. (2020). Loss of bacterial cell pole stabilization in *Caulobacter*
887 *crescentus* sensitizes to outer membrane stress and peptidoglycan-directed
888 antibiotics. *Mbio*, *11*(3), e00538-20.
889
890 Van der Ploeg, R., Goudelis, S. T., & Den Blaauwen, T. (2015). Validation of FRET
891 assay for the screening of growth inhibitors of *Escherichia coli* reveals elongasome
892 assembly dynamics. *International journal of molecular sciences*, *16*(8), 17637-17654.
893
894 Wang, D., Xue, H., Wang, Y., Yin, R., Xie, F., & Luo, L. (2013). The *Sinorhizobium*
895 *meliloti ntrX* gene is involved in succinoglycan production, motility, and symbiotic
896 nodulation on alfalfa. *Applied and environmental microbiology*, *79*(23), 7150-7159.
897
898 Werner, J. N., Chen, E. Y., Guberman, J. M., Zippilli, A. R., Irgon, J. J., & Gitai, Z.
899 (2009). Quantitative genome-scale analysis of protein localization in an asymmetric
900 bacterium. *Proceedings of the National Academy of Sciences*, *106*(19), 7858-7863
901
902 Wu, C. F., Lin, J. S., Shaw, G. C., & Lai, E. M. (2012). Acid-induced type VI secretion
903 system is regulated by ExoR-ChvG/ChvI signaling cascade in *Agrobacterium*
904 *tumefaciens*. *PLoS Pathog.* 8, e1002938
905
906
907
908

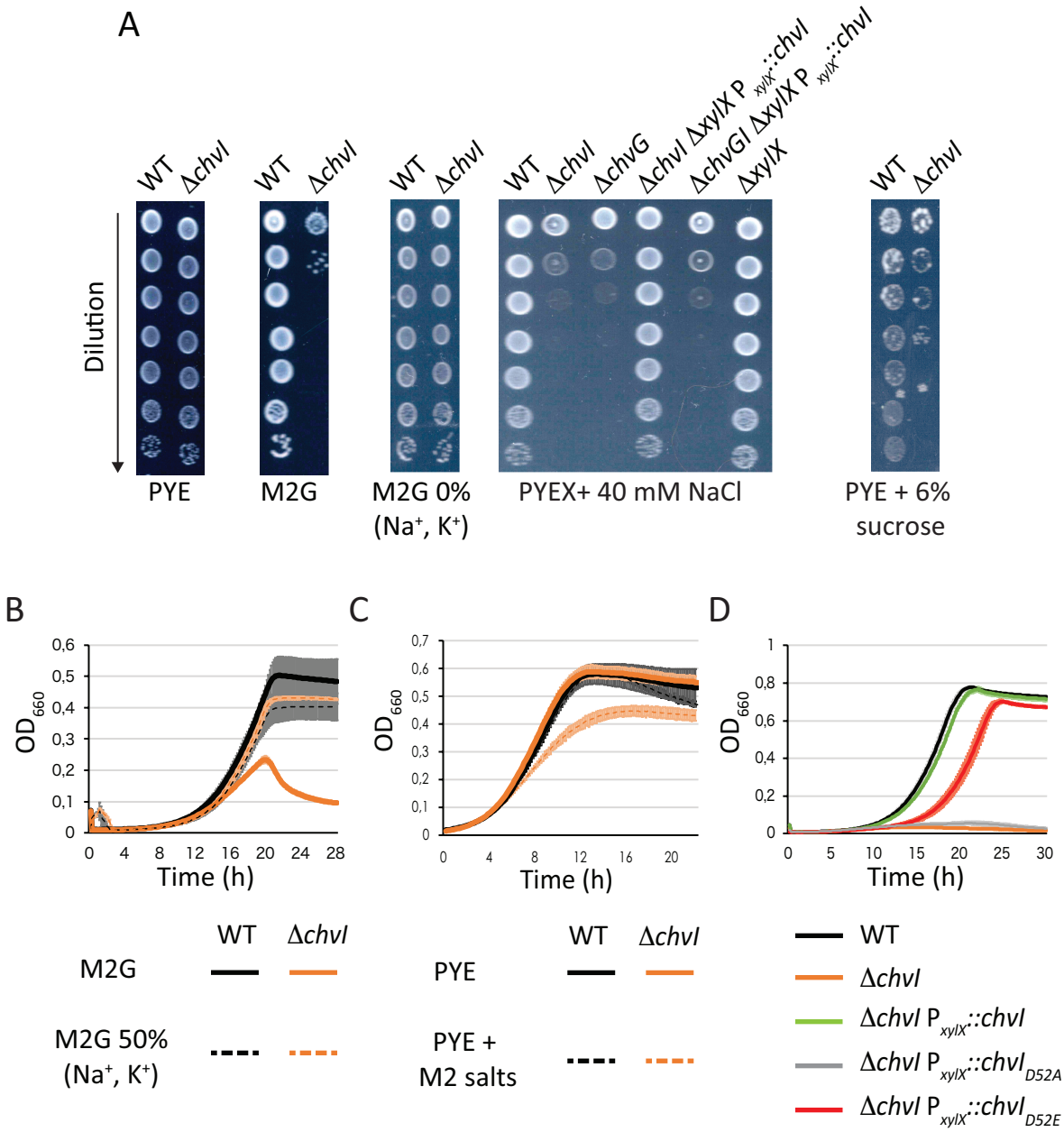

Fig. 1. Viability and growth of *chvGI* mutants in hyperosmotic conditions. (A) Viability of WT and Δ*chvI* cells in complex (PYE) and synthetic minimal media (M2G) plates with varying osmolytes concentrations. For complementation assays, PYE was supplemented with 0.1% xylose (PYEX). (B) Growth in minimal media with 100% (solid lines) or 50% (dashed lines) Na_2HPO_4 and KH_2PO_4 concentrations referred to M2G. (C) Growth in PYE supplemented with 1X M2 salts. (D) Growth in M2G of mutants complemented with WT, phospho-ablative (*chvI*$_{D52A}$) or phospho-mimetic (*chvI*$_{D52E}$)

917 mutants of *chvI* expressed from the xylose-inducible promoter P_{xylX}. Data from (B) to
918 (D) represent the average value of biological replicates (n=3, error bars show standard
919 deviation). WT and Δ*chvI* mutant are represented in (B) to (D) in black and orange,
920 respectively.
921

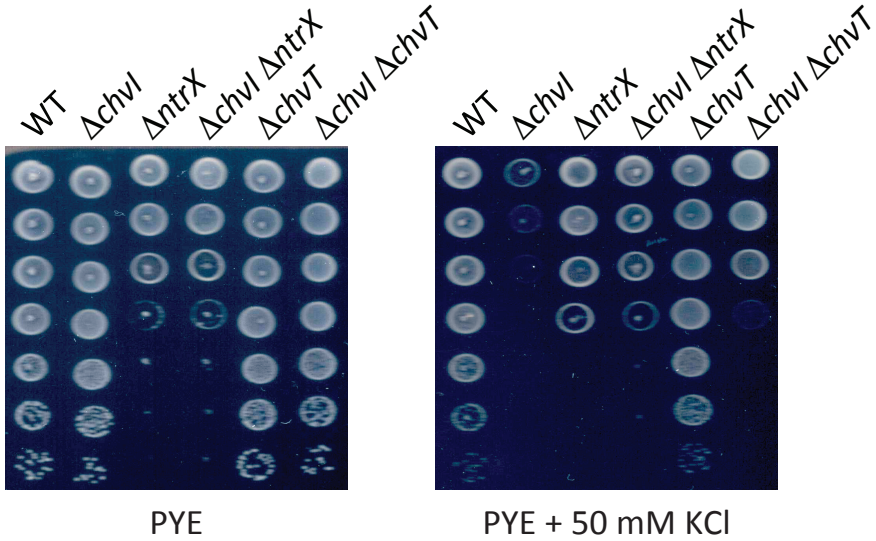

922
923
924 **Fig. 2. Growth and viability of *chvI*, *chvT* and *ntrX* mutants in hypertonic**
925 **conditions.** Viability of single (Δ*chvI*, Δ*chvT* and Δ*ntrX*) and double (Δ*chvI* Δ*chvT* and
926 Δ*chvI* Δ*ntrX*) mutants on PYE agar with or without 50 mM KCl. Images represent three
927 biological replicates.
928

A

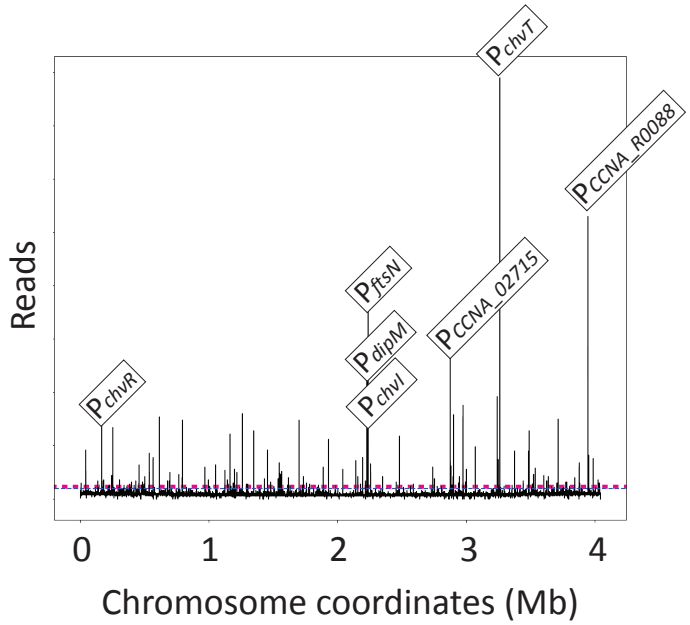
PchvT
PCCNA_R0088
PftsN
PdipM
PchvI
PCCNA_02715
PchvR
Reads
0
1
2
3
4
Chromosome coordinates (Mb)

B

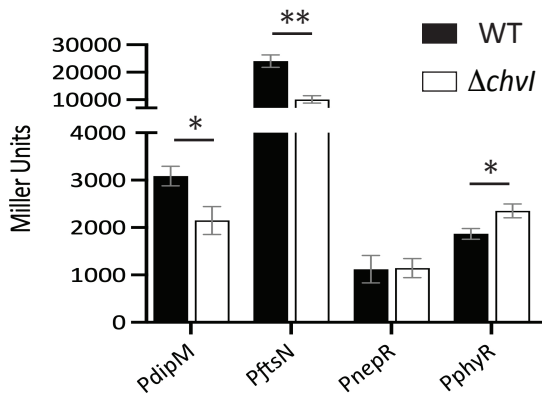
WT
ΔchvI
Miller Units
30000
20000
10000
4000
3000
2000
1000
0
*
**
*
PdipM
PftsN
PnepR
PphyR

C

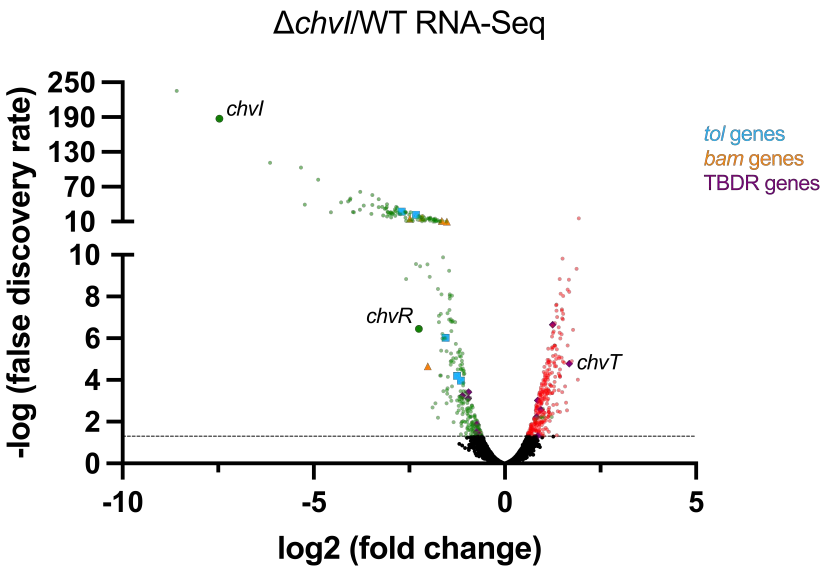
ΔchvI/WT RNA-Seq
-log (false discovery rate)
250
190
130
70
10
10
8
6
4
2
0
chvI
chvR
chvT
tol genes
bam genes
TBDR genes
-10
-5
0
5
log2 (fold change)

929

930

931 **Fig. 3. ChvI target genes determined by ChIP-seq and validated by β-**
932 **galactosidase assays**. (A) Genome-wide occupancy of ChvI on the chromosome of
933 *C. crescentus* determined by ChIP-seq on WT strain grown in M2G. The x-axis
934 represents the coordinates on the genome (Mb), the y-axis shows the normalized
935 ChIP-Seq read abundance in reads. Some top hits, corresponding to the promoter
936 regions of *chvT*, *CCNA_R0088*, *ftsN, CCNA_02715*, *chvR*, *dipM* and *chvI* operon, are
937 highlighted. (B) Activity of the *dipM*, *ftsN*, *nepR* and *phyR* promoters (Miller Units) in
938 WT (black bars) and Δ*chvI* (white bars) cells grown O.N in PYE, then washed and
939 exposed for 4h in M2G. The data represent the average values of biological replicates
940 (n=3, error bars show standard deviation). * = $p < 0.05$, ** = $p < 0.01$, single factor
941 ANOVA analysis of β-galactosidase activity. C. Volcano plot representing the relation
942 between the fold change and P values on gene expression between Δ*chvI* and WT
943 strains exposed to osmotic upshift in PYE 6% sucrose by RNA-seq. Genes identified
944 are presented as dots. Significant down- and up-regulated genes are presented as
945 green and red dots, respectively, while genes with no significant alterations are
946 presented as black dots. *chvI, chvR* and *chvT* genes as well as genes encoding Tol
947 (blue) and Bam (orange) complexes or TonB-dependent receptors (purple) are
948 highlighted.

949

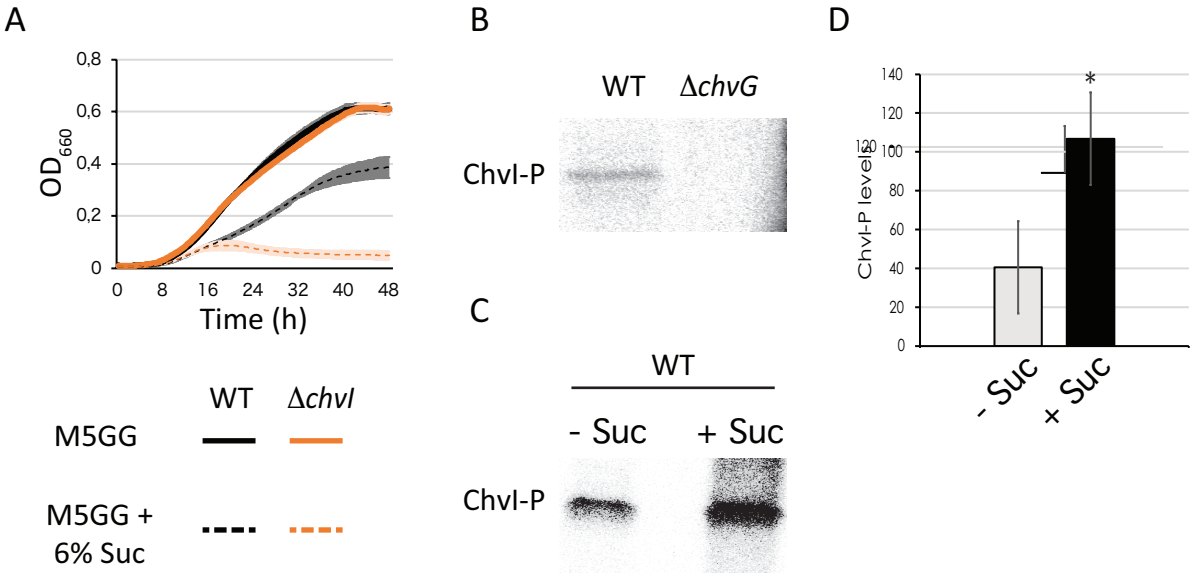

Fig. 4. ChvG-dependent phosphorylation of ChvI is stimulated upon osmotic shock. (A) Growth of WT (black) and Δ*chvI* mutant (orange) in M5GG with (dashed lines) or without (solid lines) 6% sucrose (Suc). The data represent the average value of biological replicates (n=3, error bars show standard deviation). (B) *In vivo* phosphorylation levels of ChvI in WT and Δ*chv*G mutant grown in M5GG. (C) *in vivo* phosphorylation levels of ChvI in WT grown in M5GG without (-) or with (+) sucrose (Suc) for 7 min. (D) Quantified *in vivo* phosphorylation levels of ChvI in the same growth conditions than in (C). The data represent the average values of biological replicates (n=3, error bars show standard deviation). * = $p < 0.05$, single factor ANOVA analysis of ChvI phosphorylation.

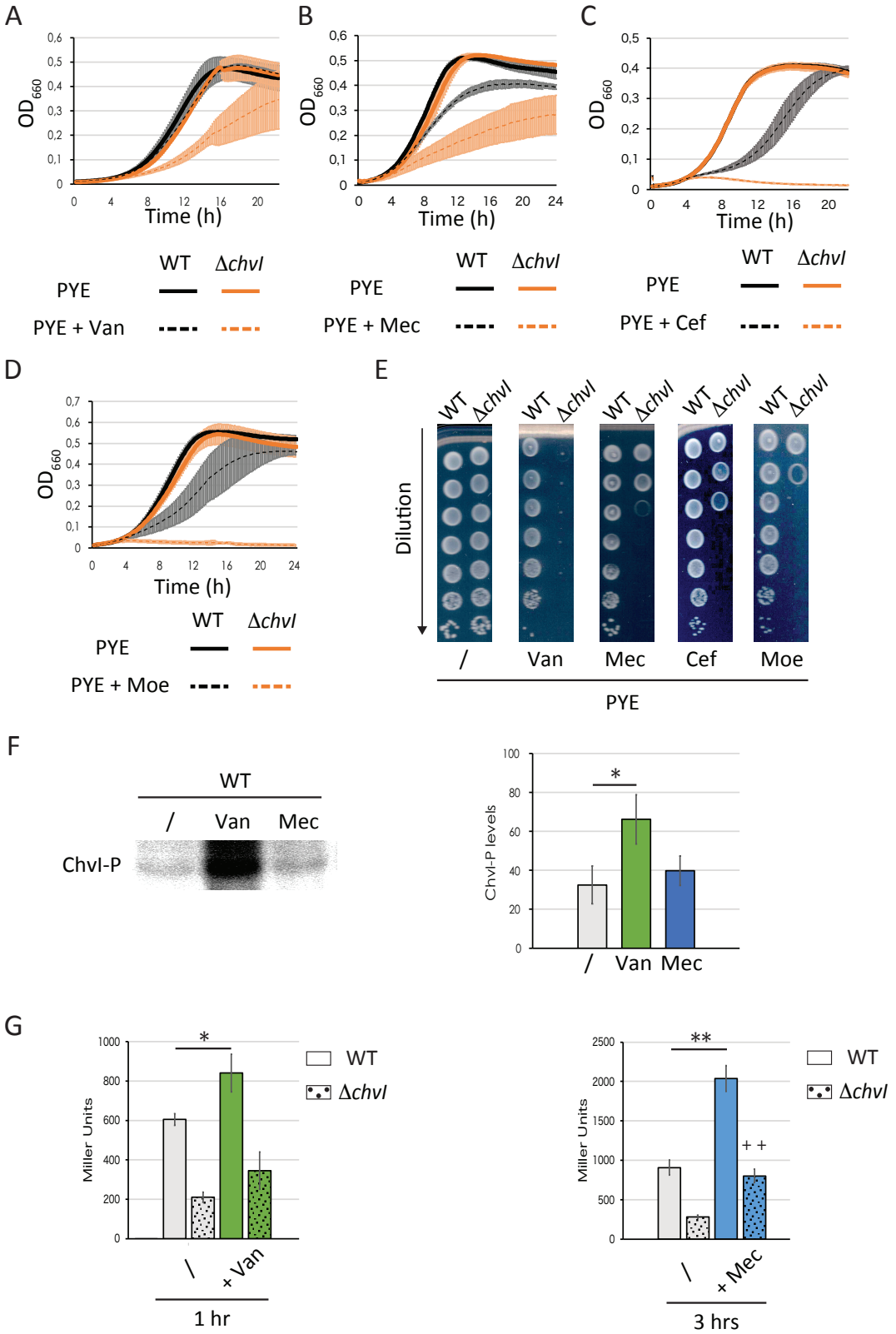
A
B
C
D
E
F
G
OD660
Time (h)
WT
ΔchvI
PYE
PYE + Van
PYE + Mec
PYE + Cef
PYE + Moe
Dilution
/
Van
Mec
Cef
Moe
ChvI-P
ChvI-P levels
Miller Units
+ Van
+ Mec
1 hr
3 hrs

963

964

965 **Fig. 5. ChvI responds to treatment with antibiotics targeting transpeptidation of**
966 **peptidoglycan during elongation (**A-D) Growth of WT and Δ*chvI* mutant cells in PYE
967 supplemented with either Vancomycin (Van) (A), mecillinam (Mec) (B), cefsulodin
968 (Cef) (C) or moenomycin (Moe) (D). (E) Viability of WT and Δ*chvI* mutant upon
969 treatment with the antibiotics indicated above. Images are representative of three
970 biological replicates. (F) Quantified *in vivo* phosphorylation levels of ChvI in WT grown
971 in M5GG without antibiotics (/) or with 10 μg/ml vancomycin (Van, green) or 100
972 μg/ml mecillinam (Mec, blue) for 7 min. (G) Activity of the *chvI* promoter P_{chvI} (in Miller
973 Units) in WT (solid bars) and Δ*chvI* (dashed bars) cells grown in minimal media M5GG
974 supplemented with antibiotics at the indicated times. The data in figures (A-D) and (F-
975 G) represent the average values of biological replicates (n=3, error bars show
976 standard deviation). * = $p < 0.05$ and ** = $p < 0.01$, and ++ = $p < 0.01$ for comparison
977 with Δ*chvI* cells using single factor ANOVA analysis. WT and Δ*chvI* mutant are
978 represented in (A) to (D) in black and orange, respectively.
979

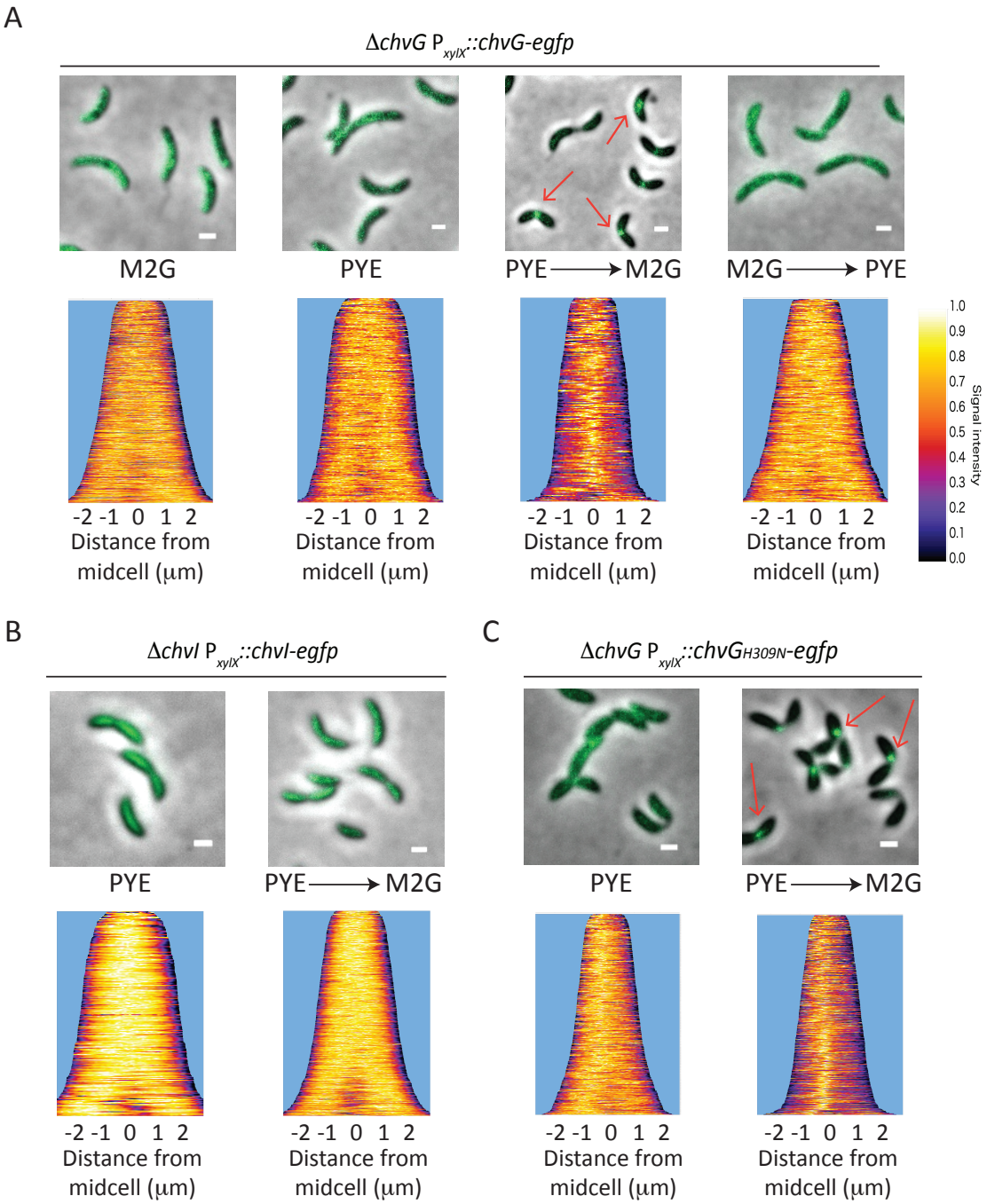

980

981

982

983

984

985 **Fig. 6. ChvG relocates from a patchy-spotty pattern to mid-cell upon osmotic**
986 **upshift.** (A) Localisation of ChvG-eGFP in cells grown in either M2G or PYE and
987 imaged on M2G or PYE agar pads, respectively; or cells grown in PYE, washed in
988 M2G and imaged on M2G agarose pads (PYE → M2G); or cells grown in M2G,
989 washed in PYE and imaged on PYE agarose pads (M2G → PYE). (B) Localisation of
990 ChvI-eGFP in a Δ*chvI* background and (C) $ChvG_{H309N}$-eGFP in a Δ*chvG* background
991 grown overnight in PYE and imaged on PYE agarose pads or grown in PYE, washed
992 in M2G and imaged on M2G agarose pads (PYE → M2G). Demograph data represent
993 cells sorted from short to long length with no less than 200 cells per sample. Liquid
994 cultures and pads were supplemented with 0.1 % xylose to allow expression of ChvG,
995 ChvI and $ChvG_{H309N}$ fused to eGFP fusions. Scale bar= 1 μm.
996

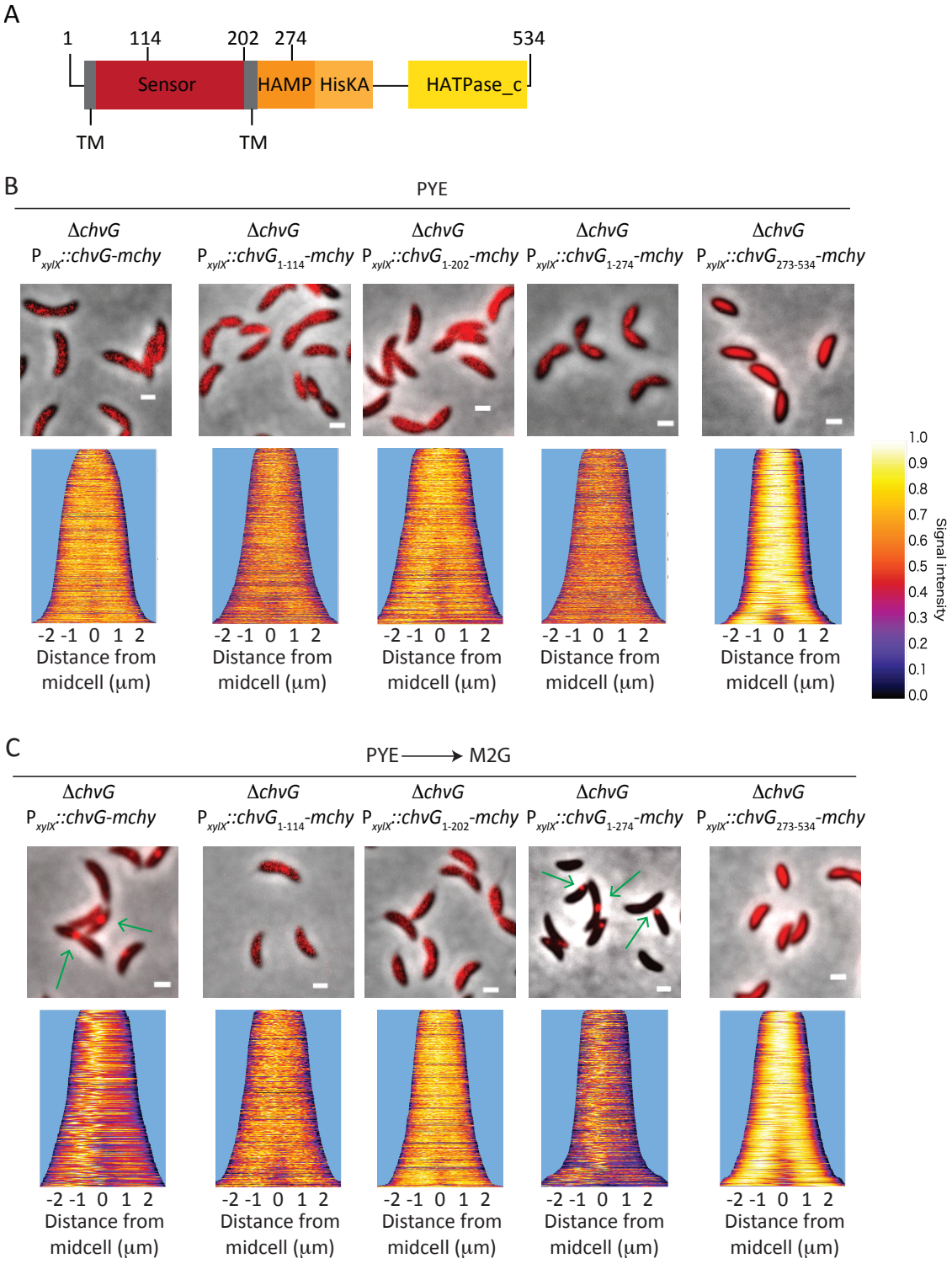
A
1
114
202
274
534
Sensor
HAMP
HisKA
HATPase_c
TM
TM
B
PYE
ΔchvG
P xylX::chvG-mchy
ΔchvG
P xylX::chvG 1-114-mchy
ΔchvG
P xylX::chvG 1-202-mchy
ΔchvG
P xylX::chvG 1-274-mchy
ΔchvG
P xylX::chvG 273-534-mchy
-2 -1 0 1 2
Distance from midcell (μm)
1.0
0.9
0.8
0.7
0.6
0.5
0.4
0.3
0.2
0.1
0.0
Signal intensity
C
PYE → M2G
ΔchvG
P xylX::chvG-mchy
ΔchvG
P xylX::chvG 1-114-mchy
ΔchvG
P xylX::chvG 1-202-mchy
ΔchvG
P xylX::chvG 1-274-mchy
ΔchvG
P xylX::chvG 273-534-mchy
-2 -1 0 1 2
Distance from midcell (μm)

1002 **Fig. 7. The N-terminal periplasmic sensor domain of ChvG is required for patchy-**
1003 **spotty localisation pattern and mid-cell relocation.** (A) Conserved domains in the
1004 HK ChvG and position of the amino acids defining the truncated proteins. (B-C)
1005 Localisation of ChvG WT and truncated versions in cells grown in PYE and imaged on
1006 PYE agarose pads (B) or in cells grown in PYE, washed in M2G and imaged on M2G
1007 agarose pads (PYE → M2G) (C). Liquid cultures and pads were supplemented with
1008 0.1 % xylose. Demograph data represent cells sorted from short to long length with no
1009 less than 300 cells per sample. Scale bars in microscopy images correspond to 1 μm.
1010